Bulletin of the Seismological Society of America, Vol. 80, No. 4, pp. 870–888, August 1990

RUPTURE PROCESS OF AN EARTHQUAKE WITH KILOMETRIC SIZE FAULT INFERRED FROM THE MODELING OF NEAR-SOURCE RECORDS

BY JEAN-CHRISTOPHE GARIEL, RALPH J. ARCHULETA, AND MICHEL BOUCHON

ABSTRACT

We use the exceptional set of strong ground motion records obtained during one of the largest aftershocks (M_L = 5.0) of the 1979 Imperial Valley earthquake to study the time history of rupture on a kilometric size fault. We apply single crack, composite cracks, and dislocation earthquake models to simulate the source and calculate the ground velocity and acceleration at the recording sites. The best fit to the data is obtained for a crack-like source where rupture is initiated at one edge and expands circularly over the fault. The stress drop inferred is 720 bars, and the fractured area has a diameter of about 1 km. The fault is vertical and strikes in the N320°E direction. This simple model explains surprisingly well the amplitudes and waveforms of the ground velocities and accelerations recorded in the near-source region during the event.

INTRODUCTION

Since the pioneering work of Aki (1968) and Haskell (1969), numerical simulations of ground motion records obtained at proximity of earthquake faults have become an important tool in investigating the rupture process of earthquakes. One important result of these studies is that relatively simple source models explain well the low-frequency part of the records obtained for several events (e.g., Heaton and Helmberger, 1978; Archuleta and Day, 1980; Bouchon, 1982; Bernard and Madariaga, 1984).

The remarkable set of near-source records obtained during one of the largest aftershocks (M_L = 5.0) of the 1979 Imperial Valley, California, earthquake allows a detailed study of the rupture history of an earthquake with kilometric-size fault. This event was studied by Liu and Helmberger (1985), who inferred it to be a complex rupture and modeled it as the superposition of two double-couple point sources having different mechanisms. We shall use here current earthquake models to simulate the source, and we shall compute the resulting ground velocity and acceleration at the recording sites. By comparing the results obtained with the observations, we shall try to discriminate between source models.

DATA

The event studied occurred at 23:19 on 15 October 1979. The hypocentral location is (Spudich and Cranswick, 1984): 32°46.39'N, 115°25.63'W, and 9.28 km depth (Fig. 1). The resulting ground accelerations were recorded by 16 accelerographs located at epicentral distances ranging from 8 to 25 km and providing a good azimuthal coverage (Porcella *et al.*, 1982).

Ground velocities obtained after integration of the accelerograms and after rotation of the horizontal traces into transverse and radial components are displayed in Figure 2. Most of the traces start during the arrival of the P-wave pulse, except for six stations (E06, E08, E09, EDA, HVP, and BCR) which were still triggered by the main shock when the aftershock occurred. The major arrival on the horizontal

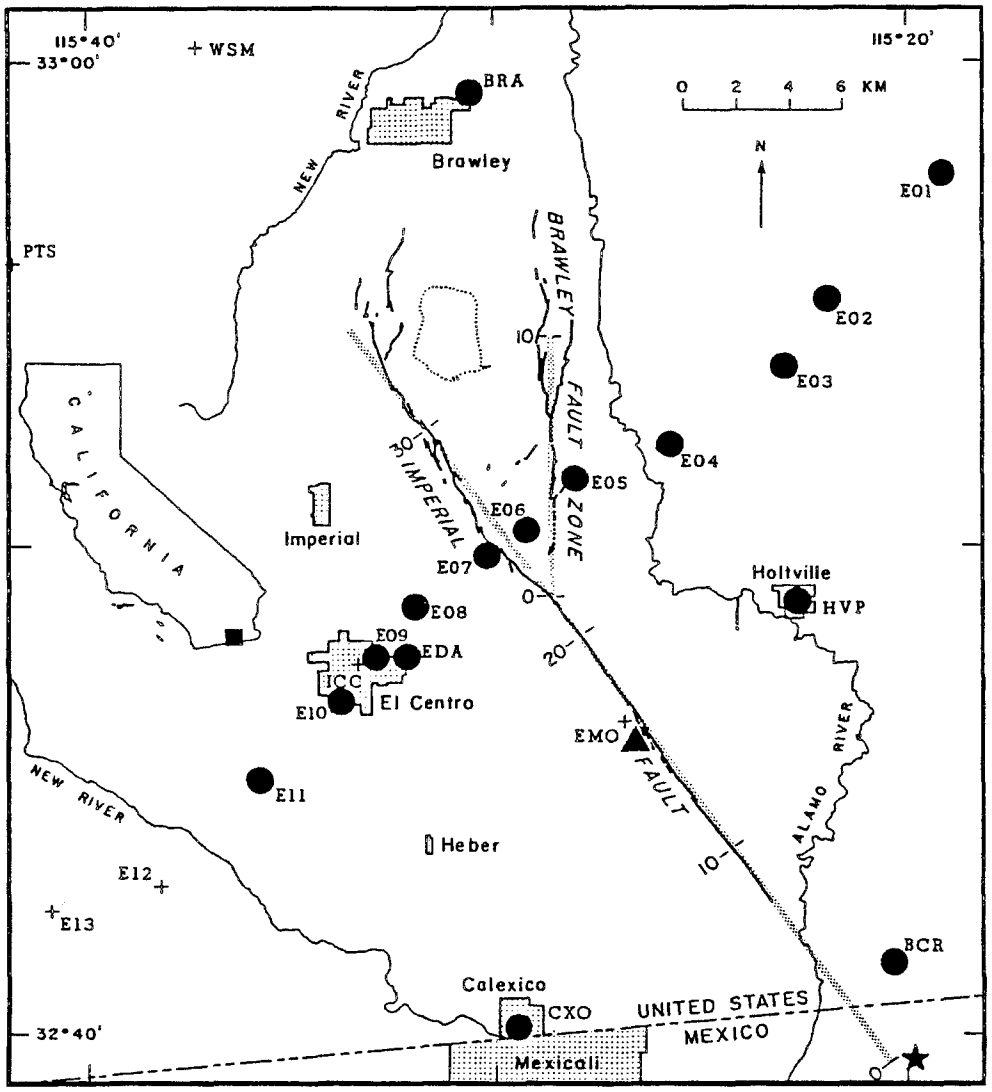

FIG. 1. Map of the Imperial Valley region (after Archuleta, 1984). The broken lines indicate the surface fractures produced by the earthquake. The epicenter of the main shock is represented by a star, and the one of the event studied by a triangle. The location of the recording stations is indicated by dots.

components corresponds to the direct S wave. Because of the low shear-wave and compressional-wave velocities near the surface (Porcella, 1984), an almost total decoupling takes place between the P- and S- wave pulses which are present only on the vertical and on the horizontal components, respectively. We shall take advantage of this decoupling and restrict the present study to the modeling of the S wave. The vertical velocity records (not shown here) are characterized by a frequency content much higher than the horizontal ones. This complex high-frequency character of the P wave is typical of near-source records obtained for strike-slip earthquakes in California. Cranswick and Muller (1985) suggest that their high frequencies partly reflect the effect of the water table, while Liu and Helmberger (1985) invoke low Q_S to explain this observation.

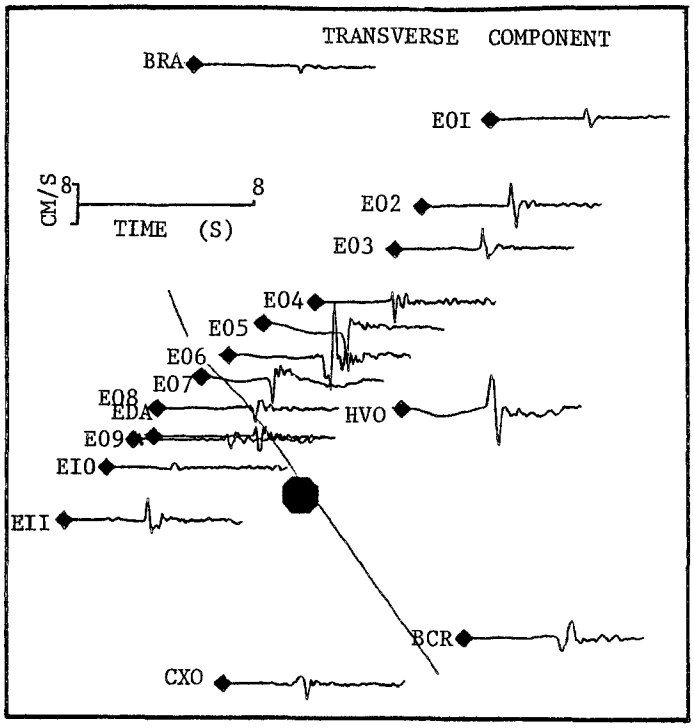

(a)

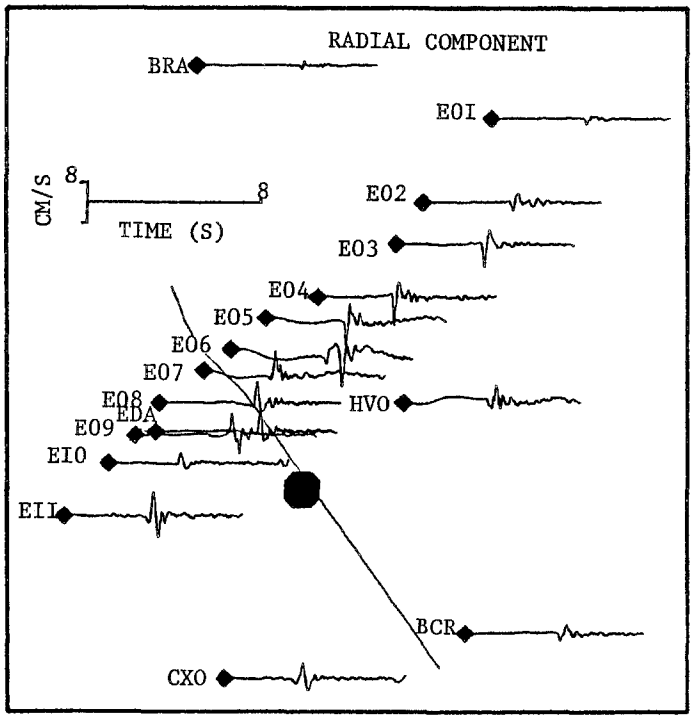

(b)

FIG. 2. Transverse (a) and radial (b) ground velocities obtained by integration of the accelerogra records.

The first-motion directions of the direct S waves in the horizontal plane are all consistent with a mechanism of right-lateral strike slip on a plane oriented approximately in the direction of the surface fault trace (N320°E to N323°E). Furthermore, the stations that are symmetrically situated with respect to the fault trace (for instance E03 and E11) have nearly equal peak horizontal amplitudes. Assuming symmetric structure, one may thus expect that the fault plane has a dip close to the vertical.

The data display a very clear directivity effect. As shown by Liu and Helmberger (1985), the width of the *SH* pulse on the transverse component presents a well marked azimuthal variation. The duration of this pulse, which is related to the rupture time, is maximum at the stations located to the southeast of the epicenter and minimum at those located to the northwest. This indicates that the rupture propagated mostly in the northwest direction.

Crustal Structure

The crustal velocity structure of the Imperial Valley region is known from an extensive refraction survey conducted in the region during 1979 (Fuis *et al.*, 1982). The data, which have been studied by McMechan and Mooney (1980) and Fuis *et al.* (1982), show that the structure around the Imperial fault is nearly tabular and that a strong velocity gradient is present in the 5 km thick sedimentary cover. Our velocity model, presented in Figure 3, is based on these studies and approximates the velocity gradient by 10 layers 500 m thick. The low, shallow shear-wave velocity considered comes from geotechnical investigations at the recording sites (Porcella, 1984).

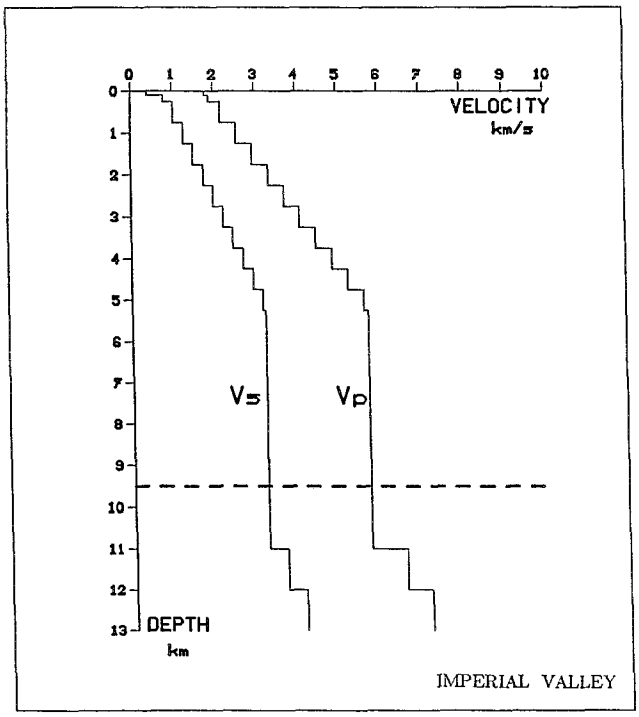

FIG. 3. Velocity model used to represent the Imperial Valley structure. This model is derived from studies by Fuis *et al.* (1982).

The Q model that we use is based on studies of spectral attenuation (Singh *et al.*, 1982; Archuleta and Bouchon, 1984):

$$0 < Z < 5 \text{ km} \qquad Q_S = 80 \qquad Q_p = 100$$

$$Z > 5 \text{ km} \qquad Q_S = 120 \qquad Q_p = 200$$

Point Source Model

We first present the solution for a point source located at the hypocentral depth (9.3 km). The method of calculation uses the discrete wavenumber representation of the wave field (Bouchon and Aki, 1977; Bouchon, 1981) combined with the reflectivity of the medium (Kennett and Kerry, 1979). We tested many different mechanisms and obtained the best fit for a right-lateral strike slip on a vertical plane oriented in the N320°E direction and for a seismic moment $M_0 = 2.0 \times 10^{23}$ dyne-cm. Except for the composite model we will use this seismic moment for each one of our source models.

The calculated transverse ground velocities are compared to the data in Figure 4. Although the amplitudes are relatively well reproduced (except for stations close to a node of radiation), the point-source model cannot describe the major characteristics of the rupture. In particular, the effects of directivity and spatial extent of the source are not present in the synthetics.

One may notice the high amplitude of synthetics at the two stations the farthest away from the source: BRA and E01. These large amplitudes are related to the arrival of the wave reflected on the interface located below the source at 11 km depth, which arrives just after the direct S wave. As this phase is absent from the data, we sligthtly modify the velocity model for the following calculations by lowering this interface to 12.5 km.

Geometry and Static Characteristics of the Rupture

Because of the small extent of the source, it is not possible to determine independently the source dimensions and the rupture velocity. The rupture duration, however, may be estimated from the width of the *SH* pulse. If we consider the pulse durations at stations E03 (0.3 s) and CXO (0.4 s) (Liu and Helmberger; 1985) located symmetrically to the northeast and southwest with respect to the source and assume a unilateral rupture propagation, one obtains a rupture duration of 0.35 sec. By combining this value with the range of rupture velocities generally accepted ($0.75V_s = 2.44$ km/s $< V_r < 0.9V_s = 2.92$ km/s, where V_s denotes the shear-wave velocity), one gets a fault length between 0.8 and 1.1 km. We shall retain a fault length of 1 km and a rupture velocity of 2.8 km/s. The choice of other values within the specified ranges would not change the results significantly.

Using the seismic moment inferred with the point-source model one then obtains the average slip on the fault:

$$D = M_0/\mu S = 86 \text{ cm}$$

This value may seem surprisingly high for an earthquake of this magnitude. We shall discuss later its implications.

Velocity Modeling

The point-source model provides quantitative estimates of the source strength and orientation but yields little information on the rupture process itself, for which

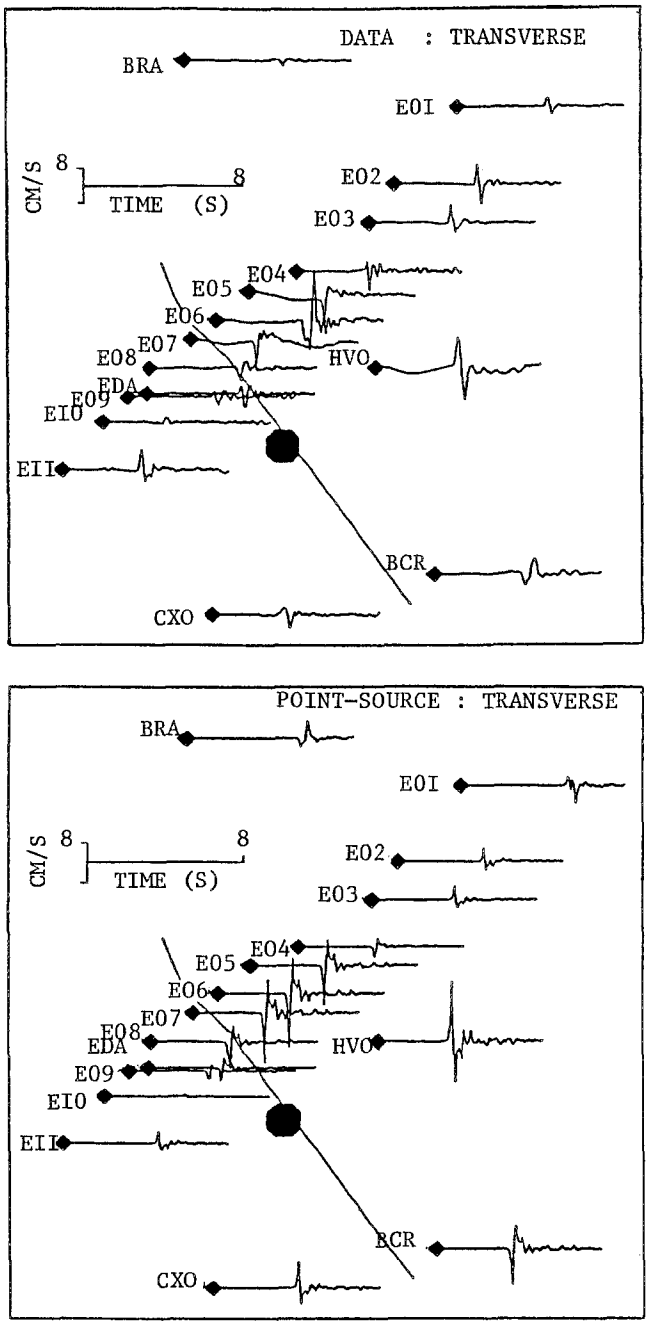

FIG. 4. Comparison between the recorded ground velocities (*top*) and the velocities calculated with the point-source model (*bottom*).

extended source models are required. We shall consider three types of extended sources: a uniform dislocation, a circular crack, and a composite model made up of several circular cracks.

In all the models considered, the rupture initiates at 9.3 km depth and takes place on a vertical plane oriented N320°E. The fault is represented by an array of 400 (20 × 20) double-couple points equally spaced at 50 m intervals in the horizontal

and vertical directions. The calculations are made for frequencies spanning the interval [0–10 Hz].

Dislocation Model

The fault is represented by a square of 1 km side. In order to account for the rupture propagation toward the northwest, the hypocenter is located at the southeast edge of the fault halfway between the shallowest and the deepest extremities of the fault. The rupture propagates radially at a velocity of 2.8 km/sec. The slip time dependence at each point of the fault is a smooth ramp function given by (Bouchon, 1981):

$$f(t) = 0.5(1 + a \tan(t/t_0))$$

The best overall fit at the 16 stations is obtained for a rise time (t_0) of 0.12 sec (Fig. 5).

Transverse Component. The agreement between the calculated and the observed amplitudes is good except at stations E05, E06, and E07. We shall leave aside station E06, which presents specific characteristics attributed to site effects (Mueller and Boore, 1981; Archuleta, 1982) for all the events recorded. As such effects are not taken into account in our simulation, we shall remove this station from the data/synthetics comparisons. The stations located in the direction of rupture propagation have a calculated amplitude larger than the observed one. This discrepancy may arise from several causes. (1) A rupture velocity too high that would increase the directivity factor. A change of rupture velocity, however, has little effect on the amplitudes because of the small spatial extent of the fault. (2) A poor determination of the mechanism. A change in the dip of the fault would mostly affect the amplitude at the stations located in the vicinity of the fault trace both in front (E05, E06, E07) and behind (CXO, BCR) the rupture. The tests carried out show that the introduction of a dip component deteriorates the fit at stations CXO and BCR. (3) An erroneous position of the hypocenter relative to the fault plane. We shall see later that a new hypocentral position yields a correct estimation of the amplitude at the stations located in the direction of rupture propagation.

The poor fit at station E04 seems to be due to another cause. This station is exactly symmetrical to station E10 with respect to the fault trace. It should thus display, like station E10, a small amplitude due to the proximity of the nodal plane. Because of the rapid amplitude variation near the nodal plane, however, this discrepancy may reflect the presence of slight lateral heterogeneities in the medium.

The agreement between calculated and observed waveforms is generally good at all the stations. The low-frequency *SH* pulses at stations CXO and BCR are well modeled.

Radial Component. The fit on the radial component is not as good as on the transverse component, as might be expected because of the possibility of converted phases. At all the stations close to nodal planes, the amplitudes of the synthetics are less than those observed on the data, as discussed above. At stations distant from nodal planes the amplitudes and waveforms are well reproduced by the synthetics.

Circular Crack Model

We now represent the faulting process as an expanding circular crack. The dynamic characteristics of this model derived from fracture physics have been

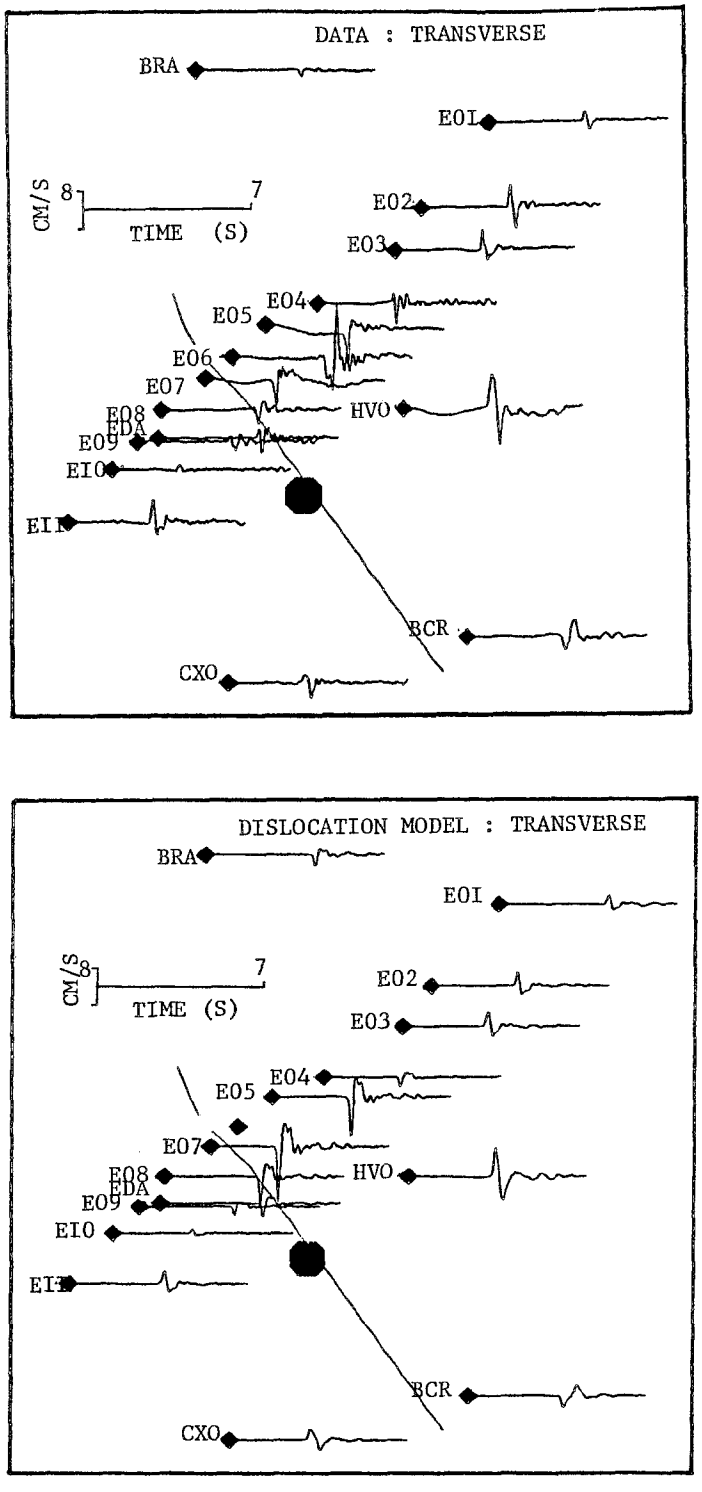

(a)

FIG. 5. (a) Comparison between the observed ground velocities (*top*) and the velocities calculated with the dislocation model (*bottom*): transverse component. (b) Comparison between the observed ground velocities (*top*) and the velocities calculated with the dislocation model (*bottom*): radial component.

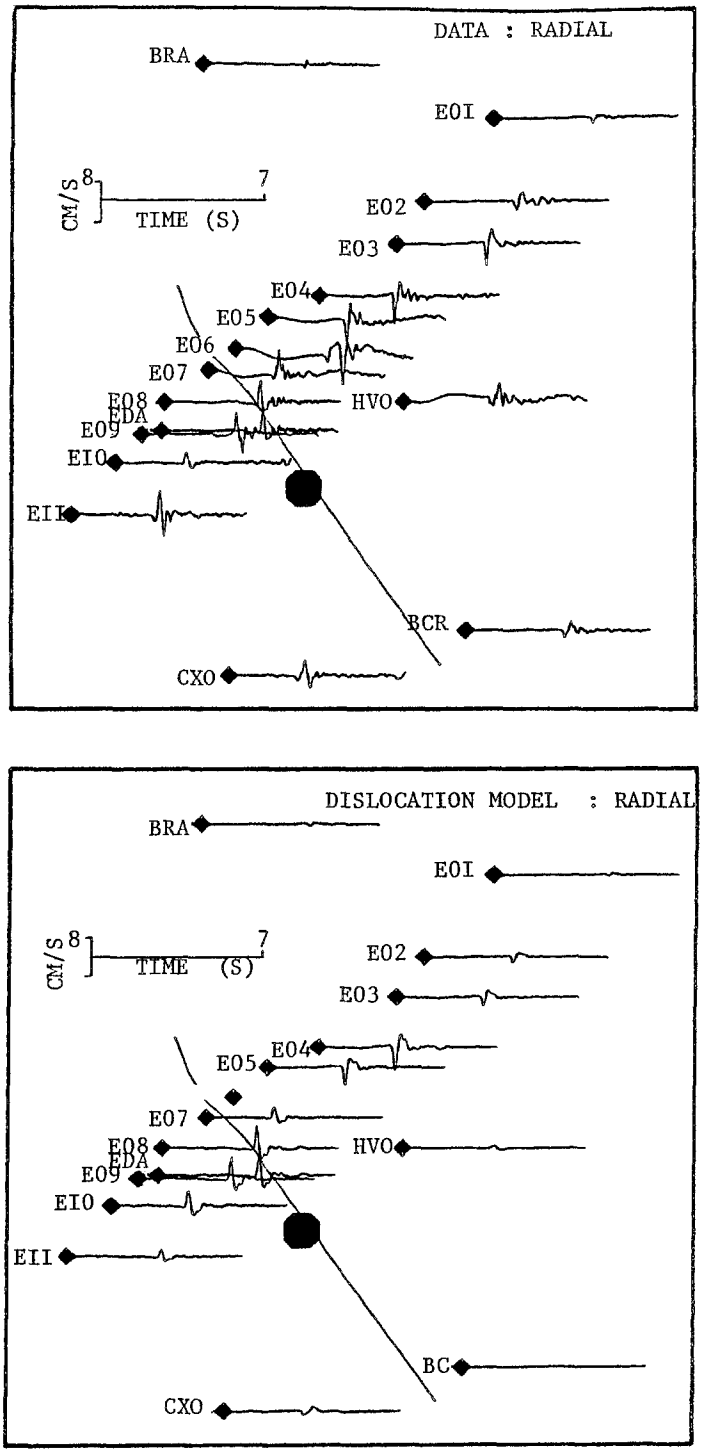

(b)

FIG. 5. (*Continued*)

obtained by Madariaga (1976) in the case where the rupture is initiated at the center of the crack, and these results have been generalized to the case of an asymmetric rupture by Virieux and Madariaga (1982). The fault-slip history inferred from these studies can be described approximately by analytical expressions. Such representations have been used to model the radiation from "crack models" of the earthquake source (Bouchon, 1978; Boatwright, 1980; Archuleta and Hartzell, 1981; Campillo, 1983).

The model is schematically represented in Figure 6. Rupture is initiated at the edge of the circular fault and propagates toward the center of the fault with a velocity v_r. At each instant the rupture front is represented by a circle. The slip D at each point of the fault is described by:

$$\frac{D(\vec{r}, t)}{D_0} = 0, \qquad t < t_0(r)$$

$$\frac{D(\vec{r}, t)}{D_0} = \sqrt{\bar{v}_r^2 t^2 - r^2}, \qquad t_0(r) < t < t_1$$

$$\frac{D(\vec{r}, t)}{D_0} = \sqrt{\bar{v}_r^2 t_1^2 - r^2}, \qquad t > t_1$$

with

$$t_0(r) = \frac{r}{\bar{v}_r} \qquad t_1 = \frac{R}{\bar{v}_r} \qquad \bar{v}_r = \frac{v_r}{2}$$

and where D_0 is the final displacement at the center of the crack and R denotes the final crack radius.

In this model, the origin of the $\vec{r}$ vector at each instant is the center of the circle representing the position of the rupture front.

The radius of the crack considered is 500 m, and the final slip at the center is taken equal to $(\frac{3}{2})D$ (dislocation) = 1.35 m, so that the crack and the dislocation

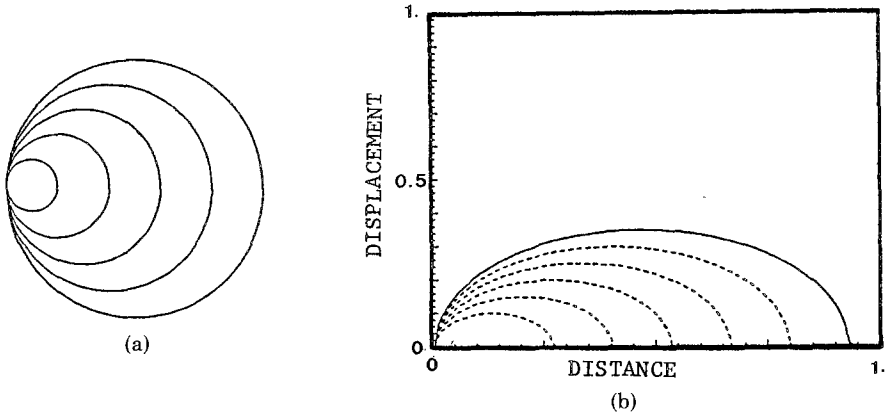

FIG. 6. (a) Geometry of the asymmetric crack model used to simulate the propagation of the rupture on the fault. The different circles represent the position of the rupture front at successive times. (b) Growth of the slip on the crack: the broken lines display the evolution of the slip at equal time intervals. The scale is arbitrary.

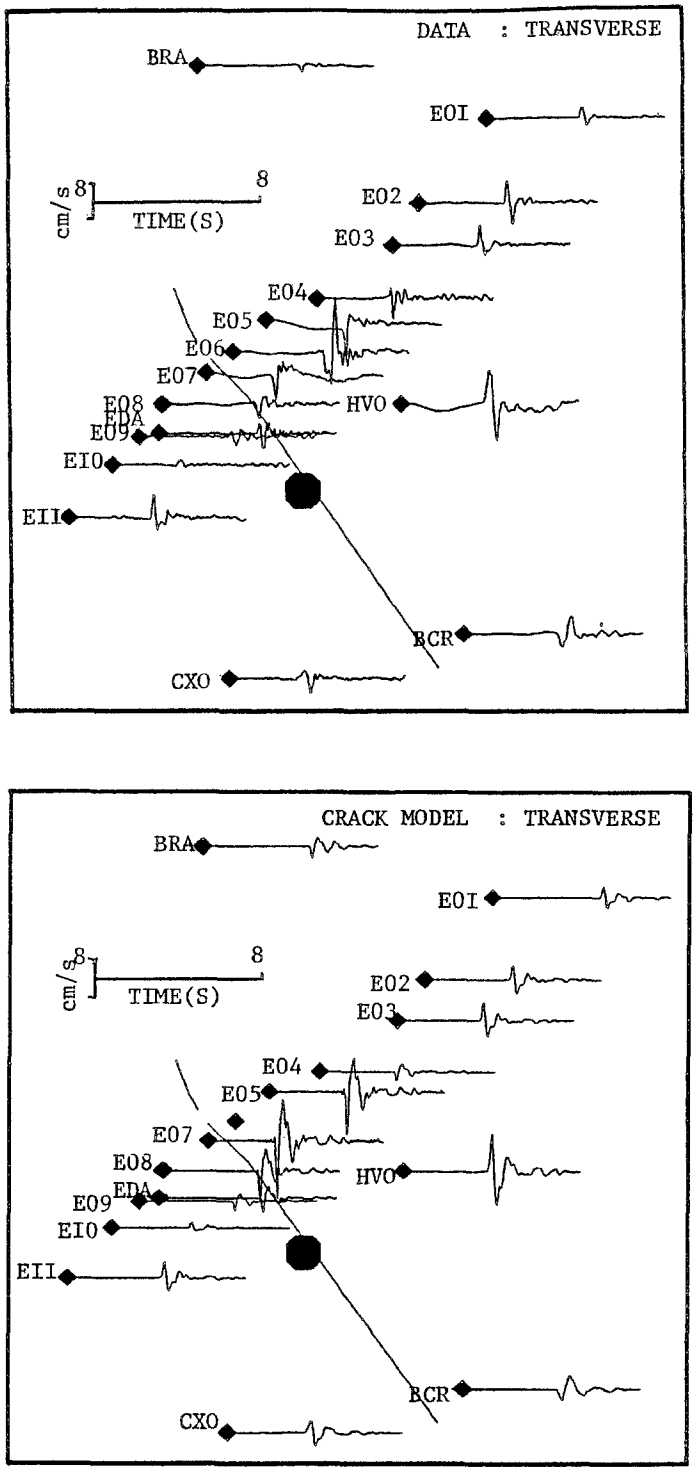

(a)

FIG. 7. (a) Comparison between the observed ground velocities (*top*) and the velocities calculated with the crack model (*bottom*): transverse component. (b) Comparison between the observed ground velocities (*top*) and the velocities calculated with the crack model (*bottom*): radial component.

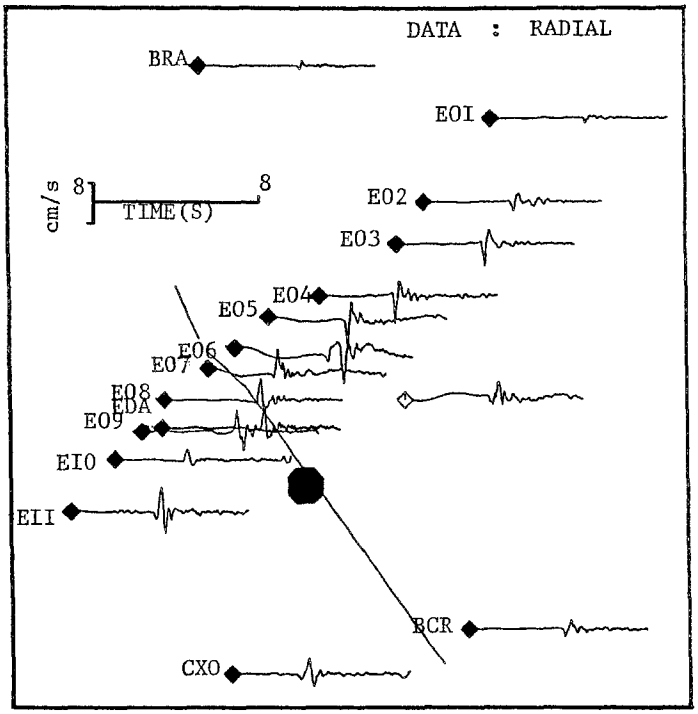

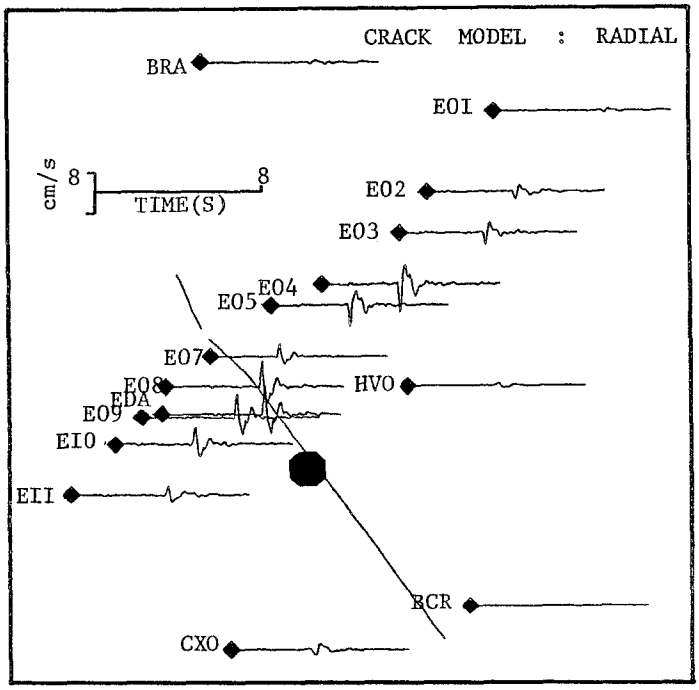

(b)

FIG. 7. (*Continued*)

models have the same seismic moment. Unlike the dislocation model, the rise time at each point of the fault is governed by the size of the source. For example, the rise time at the center of the fault is equal to 0.35 sec. The horizontal velocities obtained are compared with the data in Figure 7a (transverse) and b (radial). The synthetics are close in both amplitude and waveform to those produced by the dislocation. This similarity is due to the small spatial extent of the source (1 km). The shortest wavelengths considered in the calculation (about 300 m) are about one third of the source dimension, so that the major difference between the two models, namely the spatial variation of the slip time function in the case of a crack, is not well described. The crack model is thus seen as a dislocation.

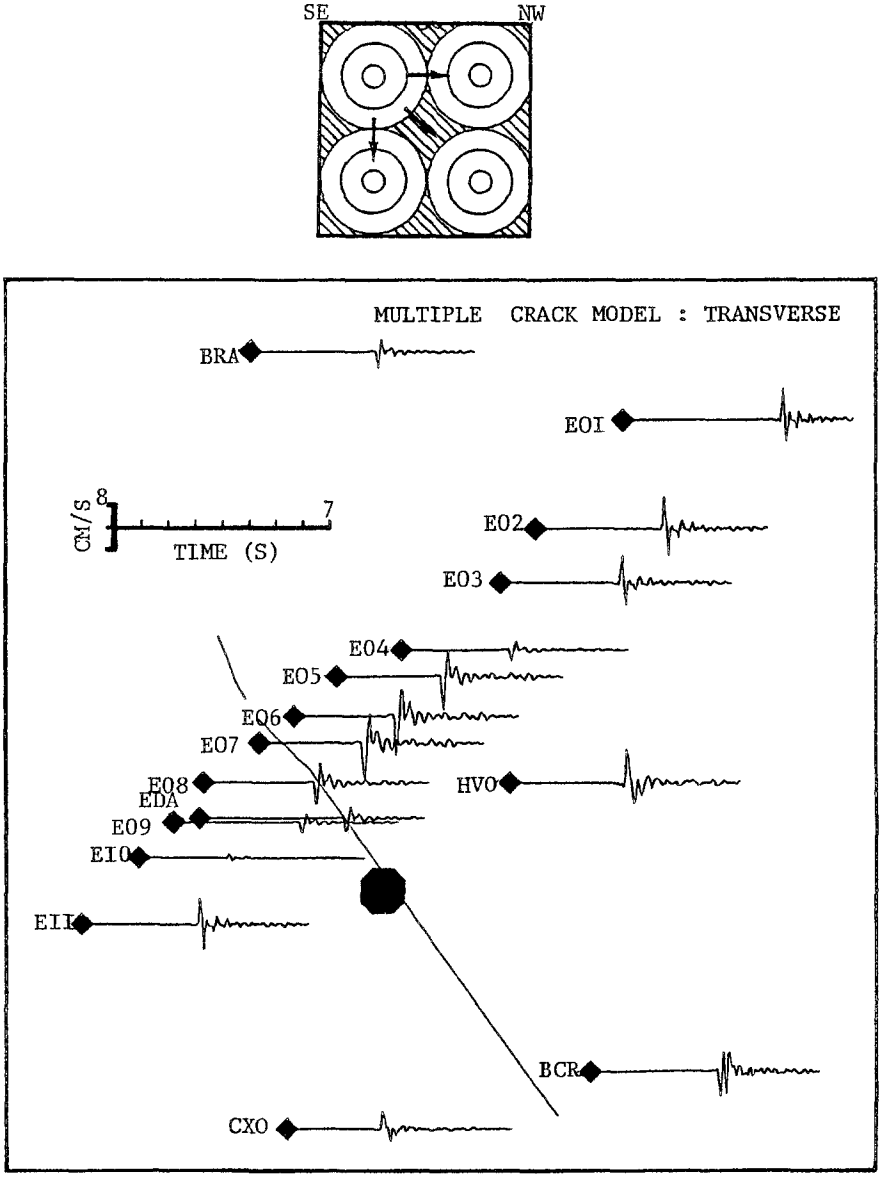

FIG. 8. Geometry of the multiple crack model considered (*top*) and resulting transverse ground velocity (*bottom*).

Composite Model

Large and intermediate size earthquakes are often described as a cascade of individual events occurring on the same fault plane within a short time span (Kanamori and Stewart, 1978; Aki, 1979). In order to test this possibility for the event studied here, we represent the source by an array of four circular cracks having a radius of 250 m each (Fig. 8). This model is based on the work of Das and Aki (1977) and Papageorgiou and Aki (1983). The rupture is initiated at the center of the upper southeastern crack and propagates radially to the other cracks at a velocity of 2.8 km/sec. The final displacement at the center of each crack is 130 cm, which corresponds to a seismic moment smaller ($M_0 = 8.10^{22}$ dyne-cm) than that of the two previous models.

The transverse velocities are presented in Figure 8. They are characterized by a higher frequency content than the previous simulations and the data. These high frequencies represent the stopping phases emitted by each crack. The individual pulses associated with these phases are clearly seen in the simulation of the station BCR.

Simulation of the Ground Acceleration

We use the circular crack model previously described (Fig. 6) to calculate the accelerations. We have observed earlier on the velocity simulations that all the models we considered overestimate the amplitudes at the stations located in the direction of rupture propagation. As the efficiency of radiation is maximum in such a direction, the location of the hypocenter on the edge of the fault must mostly influence the amplitude at the northwestern stations. For this reason we tested three hypocentral locations (Fig. 9a). The transverse accelerations produced at stations E05 and BCR for these three positions are shown in Figure 9b. The best

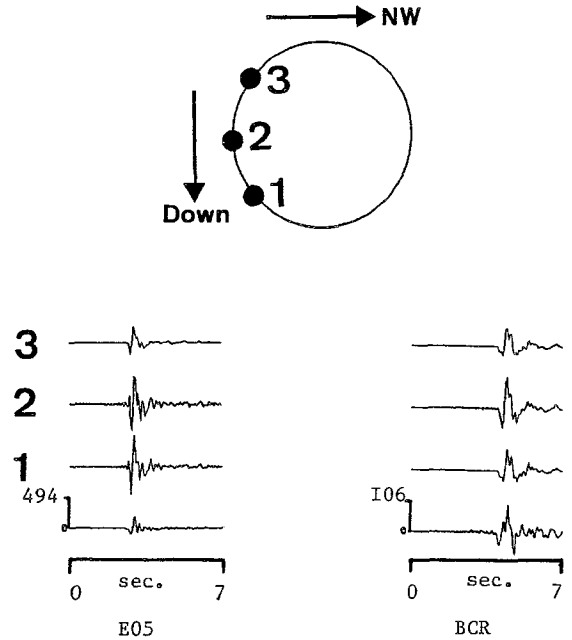

FIG. 9. Comparison of the transverse accelerations calculated for three hypocentral positions with the observed accelerations at stations E05 and BCR.

trade-off in amplitude between these two stations located in widely different azimuths corresponds to an hypocentral location in the upper part of the fault (hypocenter 3).

The transverse and radial ground accelerations calculated with this model are compared in Figure 10 with the data low-pass filtered below 10 Hz. On the transverse component, the fit in amplitude is good at all the stations except E04, which is located near a nodal plane. The directivity effect on peak accelerations is well reproduced. The acceleration waveforms and amplitudes are remarkably well simulated at stations HVP and E11 on the transverse component. These two stations are located almost normally to the fault with respect to the source. This provides them the "best view" of the rupture process and a least sensitivity to directivity. Moreover, these two are the ones for which the seismic rays travel the shortest distance in the fault zone, a region likely to be heterogeneous.

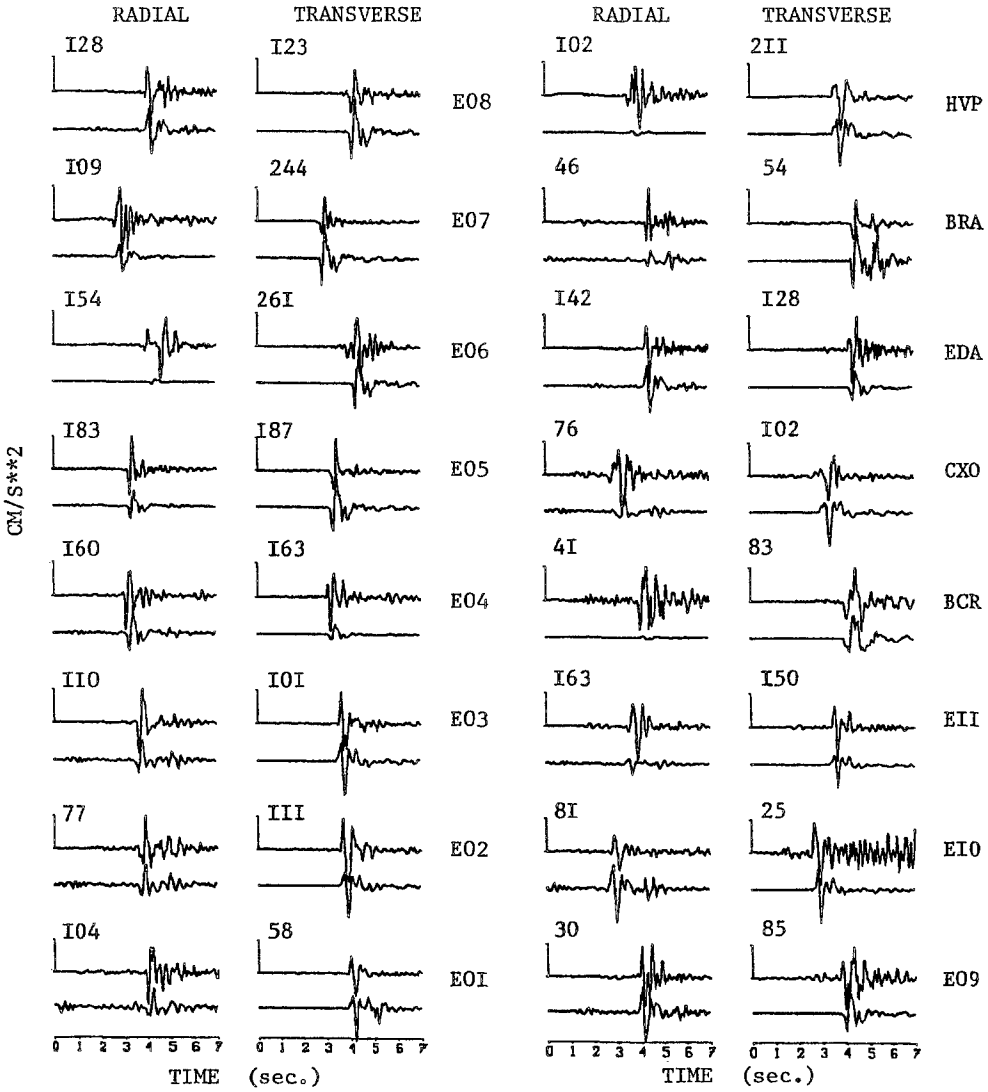

FIG. 10. Comparison between the recorded accelerations low-pass filtered at 10 Hz (upper traces) and the accelerations produced by the crack model (lower traces).

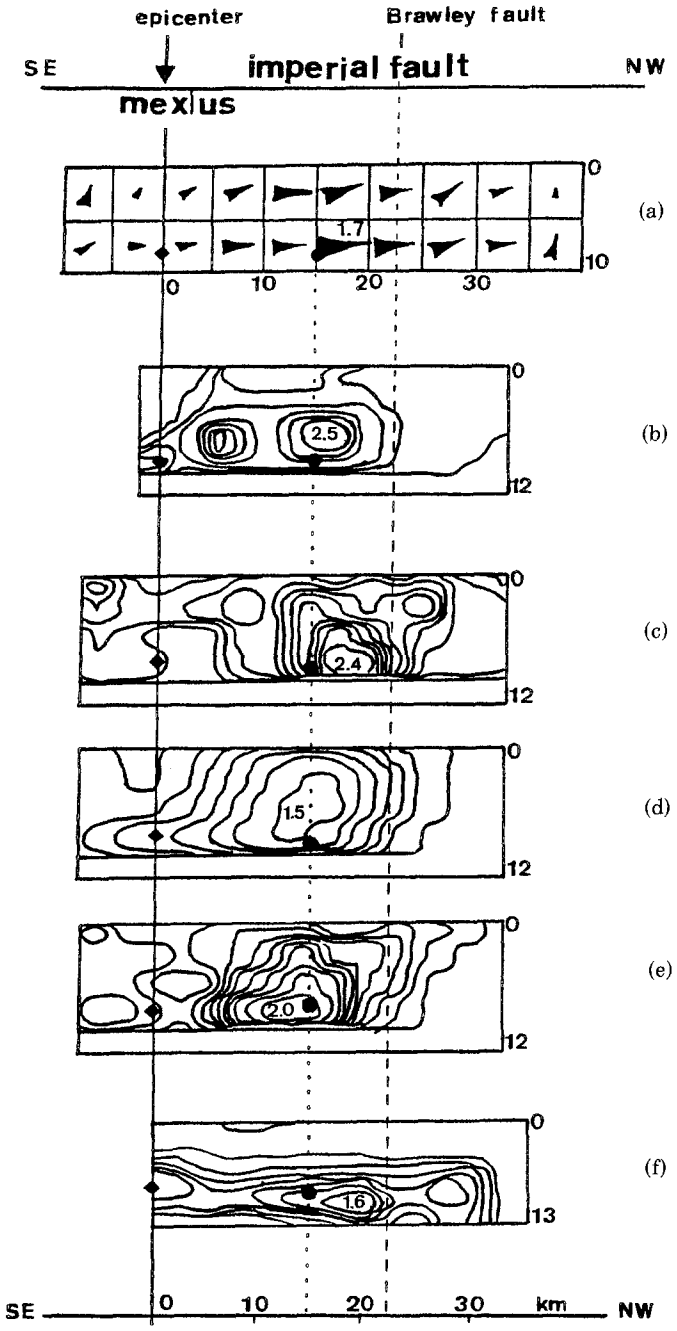

FIG. 11. Results of the different inversions of fault slip performed for the Imperial Valley earthquake. The position of the event is indicated on each drawing by a black dot (after Bernard, 1987). a: Olson and Apsel (1982); b: Hartzell and Helmberger (1982); c, d, e: Hartzell and Heaton (1983), f: Archuleta (1984).

On the radial component, the agreement is not as good as for the transverse component for the reasons previously discussed.

DISCUSSION AND CONCLUSION

This study shows that a very localized crack-like rupture occurring on the Imperial fault (strike = N320°E, dip = 90°) and extending over an area of about 1 km^2,

associated with an average slip of approximately 90 cm, explains the horizontal accelerations recorded at 16 stations around the fault.

The aftershock studied is located on the Imperial fault, in a zone where all the inversion results obtained for the main shock (Olson and Apsel, 1982; Hartzell and Helmberger, 1982; Hartzell and Heaton, 1983; Archuleta, 1984) indicate that large fault slip occurred during the earthquake (Fig. 11). This would imply that, in this zone, the stress drop caused by the main shock was relatively high. Hartzell and Helmberger (1982), for instance, estimate it at 200 bars. In this context, our event would correspond to a very localized area of higher strength which was not immediately broken at the passage of the rupture front of the earthquake. The stress relaxation around this part of the fault would then have resulted in a local increase of the tectonic stress, which would have led rapidly to the rupture. It thus seems logical that the fault slip associated with the aftershock is of the same order as the one which took place during the main shock. It is possible to estimate the corresponding stress drop:

$$\Delta\sigma = \frac{7\pi}{24}\mu\frac{D_0}{R} = 720 \text{ bars}$$

The major results of this study are (1) the source of the event considered is surprisingly simple in the frequency range [0–10 Hz], and (2) the ground velocities and accelerations produced can be simulated numerically by representing the fault as a unique crack-like rupture.

Using an extended source, it is not necessary to invoke, as did Liu and Helmberger (1985), a combination of two lagged point sources with a change in mechanism. Moreover, our mechanism is in agreement with the one determined by Zollo and Bernard (1989) using a polarization inversion technique.

Because of the small spatial extent of the fault, this data set does not resolve the issue of whether the crack model or the dislocation model is a better representation of the source. Discrimination between crack model and dislocation model would require near-source data from intermediate or large size earthquakes.

ACKNOWLEDGMENTS

Most of the calculations presented in this article were performed at the Centre de Calcul Vectoriel pour la Recherche.

REFERENCES

Aki, K. (1968). Seismic displacement near a fault, *J. Geophys. Res.* **73,** 5359–5376.

Aki, K. (1979) Characterization of barriers on an earthquake fault, *J. Geophys. Res.* **84,** 6140–6148.

Archuleta, R. J. (1982). Analysis of near-source static and dynamic measurements from the 1979 Imperial Valley earthquake, *Bull. Seism. Soc. Am.* **72,** 1927–1956.

Archuleta, R. J. (1984). A faulting model for the 1979 Imperial Valley earthquake, *J. Geophys. Res.* **89,** 4559–4585.

Archuleta, R. J. and M. Bouchon, (1984). *Earthquake Notes* **55,** 24.

Archuleta, R. J. and S. M. Day (1980). Dynamic rupture in a layered medium: the 1966 Parkfield earthquake, *Bull. Seism. Soc. Am.* **70,** 671–689.

Archuleta, R. J. and S. H. Hartzell (1981). Effects of fault finiteness on near source ground motion, *Bull. Seism. Soc. Am.* **71,** 937–957.

Bernard, P. (1987). Du caractere complexe et agressif des sources sismiques, *Ph.D. Thesis,* Université de Paris VII.

Bernard, P. and R. Madariaga (1984). A new asymptotic method for the modeling of near-field accelerograms, *Bull. Seism. Soc. Am.* **74,** 539–557.

Boatwright, J. (1980). A spectral theory for circular seismic sources: simple estimates of source dimension, dynamic stress drop and radiated seismic energy, *Bull. Seism. Soc. Am.* **70,** 1–28.

Bouchon, M. (1978). A dynamic fault model for the San Fernando earthquake, *Bull. Seism. Soc. Am.* **68,** 1555–1576.

Bouchon, M. (1981). A simple method to calculate Green's functions for an elastic layered medium, *Bull. Seism. Soc. Am.* **71,** 959–971.

Bouchon, M. (1982). The rupture mechanism of the Coyote Lake earthquake of 6 August 1969 inferred from near-field data, *Bull. Seism. Soc. Am.* **72,** 745–757.

Bouchon, M. and K. Aki (1977). Discrete wave-number representation of seismic wavefields, *Bull. Seism. Soc. Am.* **67,** 259–277.

Campillo, M. (1983). Numerical evaluation of near-field high-frequency radiation from quasi-dynamic circular faults, *Bull. Seism. Soc. Am.* **73,** 723–734.

Cranswick, E. and C. S. Muller (1985). High-frequency vertical particle motions in the Imperial Valley and *SV* to *P* coupling: the site response of the differential array and the "greenhouse effect," *Trans. Am. Geophys. Union* **66,** 968.

Das, S. and K. Aki (1977). Fault planes with barriers: a versatile earthquake model, *J. Geophys. Res.* **82,** 5648–5670.

Fuis, G. S., W. D. Mooney, J. H. Healy, G. A. McMechan, and W. J. Lutter (1982). Crustal structure of the Imperial Valley region, in *The Imperial Valley, California, Earthquake of October 15, 1979, U.S. Geol. Surv. Profess. Paper 1254,* 25–50.

Hartzell, S. H. and D. V. Helmberger (1982). Strong motion modeling of the Imperial Valley earthquake of 1979, *Bull. Seism. Soc. Am.* **72,** 571–596.

Hartzell, S. H. and T. H. Heaton (1983). Inversion of strong motion and teleseismic waveform data for the fault rupture history of the 1979 Imperial Valley, California earthquake, *Bull. Seism. Soc. Am.* **72,** 571–596.

Haskell, N. A. (1969). Elastic displacements in the near-field of a propagating fault, *Bull. Seism. Soc. Am.* **59,** 865–908.

Heaton, T. H. and D. V. Helmberger (1978). Predictability of strong ground motion in the Imperial Valley: modeling the *M* 4.9, November 4, 1976 Brawley earthquake, *Bull. Seism. Soc. Am.* **68,** 31–48.

Kanamori, H. and G. S. Stewart (1978). Seismological aspects of the Guatemala earthquake of February 4, 1976, *J. Geophys. Res.* **83,** 3427–3434.

Kennett, B. L. N. and N. J. Kerry (1979). Seismic waves in a stratified half-space, *Geophys. J. R. Astr. Soc.* **57,** 557–583.

Liu, H. L. and D. V. Helmberger (1985). The 23:19 aftershock of the October 1979 Imperial Valley earthquake: more evidence for an asperity, *Bull. Seism. Soc. Am.* **75,** 689–708.

Madariaga, R. (1976). Dynamics of an expanding circular fault, *Bull. Seism. Soc. Am.* **66,** 639–666.

McMechan, G. A. and D. W. Mooney (1980). Asymptotic ray theory and synthetic seismograms for laterally varying structures: theory and application to the Imperial Valley, California, *Bull. Seism. Soc. Am.* **70,** 2035–2121.

Mueller, C. S. and D. M. Boore (1981). Site amplification at El Centro strong motion array station No. 6, *Earthquake Notes* **52,** 84.

Olson, A. H. and R. J. Apsel (1982). Finite faults and inverse theory with applications to the 1979 Imperial Valley earthquake, *Bull. Seism. Soc. Am.* **72,** 1969–2001.

Papageorgiou, A. S. and K. Aki (1983). A specific barrier model for the quantitative description of inhomogeneous faulting and the prediction of strong ground motion: I. description of the model, *Bull. Seism. Soc. Am.* **73,** 693–722.

Porcella, R. L. (1984). Geotechnical investigations at strong-motion stations in the Imperial Valley, California, *U.S. Geol. Surv., Open-File Rept. 84–562,* 1–174.

Porcella, R. L., R. B. Matthiesen, and R. P. Malley (1982). Strong-motion data recorded in the United States, in *The Imperial Valley, California, Earthquake of October 15, 1979, U.S. Geol. Surv. Profess. Paper 1254,* 289–318.

Singh, S. K., R. Apsel, and J. N. Brune (1982). Spectral attenuation of *SH* waves along the Imperial fault, *Bull. Seism. Soc. Am.* **72,** 2003–2016.

Spudich, P. K. P. and E. Cranswisk (1984). Direct observation of rupture propagation during the 1979 Imperial Valley earthquake using a short baseline accelerometer array, *Bull. Seism. Soc. Am.* **74,** 2083–2114.

Virieux, J. and R. Madariaga (1982). Dynamic faulting studied by a finite difference method, *Bull. Seism. Soc. Am.* **72,** 345–369.

Zollo, A. and P. Bernard (1989). S-wave polarization inversion of the 15 October 1979, 23:19 Imperial Valley aftershock: evidence for anisotropy and a simple source mechanism, *Geophys. Res. Lett.* **16,** 1047–1050.

LABORATOIRE DE GEOPHYSIQUE INTERNE ET
TECTONOPHYSIQUE
UNIVERSITÉ JOSEPH FOURIER
BP53X, 38041 GRENOBLE, FRANCE
(J.-C.G., M.B.)

LAMONT-DOHERTY GEOLOGICAL OBSERVATORY
COLUMBIA UNIVERSITY
PALISADES, NEW YORK 10964
(J.-C.G.)

DEPARTMENT OF GEOLOGICAL SCIENCES
UNIVERSITY OF CALIFORNIA AT SANTA BARBARA
SANTA BARBARA, CALIFORNIA 93106
(R.J.A.)

Manuscript received 14 March 1989